Chemical Physics Letters 509 (2011) 186–191

Contents lists available at ScienceDirect

Chemical Physics Letters

journal homepage: www.elsevier.com/locate/cplett

EASY-GOING DUMBO on-spectrometer optimisation of phase modulated homonuclear decoupling sequences in solid-state NMR

Dennis L.A.G. Grimminck [a], Suresh K. Vasa [a], W. Leo Meerts [a], Arno P.M. Kentgens [a,*], Andreas Brinkmann [b]

[a] Radboud University, Institute for Molecules and Materials, Heyendaalseweg 135, NL-6525 AJ Nijmegen, The Netherlands
[b] Steacie Institute for Molecular Sciences, National Research Council, 1200 Montreal Road, M-40 Ottawa, ON, Canada K1A 0R6

ARTICLE INFO

Article history:
Received 27 October 2010
In final form 25 April 2011
Available online 3 May 2011

ABSTRACT

A one-step many-parameter optimisation scheme for phase modulated proton homonuclear decoupling sequences in solid-state NMR is presented. Phase modulations, parameterised by DUMBO Fourier coefficients, were optimised using a Covariance Matrix Adaptation Evolution Strategies algorithm. Our method, denoted EASY-GOING DUMBO, starts with featureless spectra and optimises proton–proton decoupling, during either proton or carbon signal detection. Optimisations at moderate sample magic angle spinning (MAS) frequencies and medium radio-frequency (rf) field strengths resulted in solutions closely resembling (e)DUMBO. Application of EASY-GOING DUMBO for optimisation at very high 680 kHz rf field strength, 12.5 kHz MAS on a 400 MHz NMR spectrometer resulted in a new solution, with competitively resolved proton spectra.

1. Introduction

Research on proton homonuclear decoupling in solid-state NMR has been receiving considerable attention in the last decade. Contemporary state of the art techniques are the Combined Rotation And Multiple Pulse Sequence (CRAMPS) methods [1]. These techniques rely on the shaping of radio-frequency (rf) pulses and the interplay between rf cycle and magic angle spinning (MAS) frequencies; considering the capabilities of contemporary NMR spectrometers a parameter space with a large degree of freedom. Two categories of approaches to find efficient homonuclear decoupling sequences can be distinguished. The first category can be considered as the 'bottom-up' approaches; starting from the theoretical description of the direct dipole–dipole interaction, an averaging scheme is developed. Typical examples are FSLG [2–4], PMLG [5–7] and $RN_n^{N/2}$ [8] sequences. These methods are effective as well as insightful in understanding the process of averaging homonuclear couplings. Their performance for large spin systems and non-ideal rf pulses is, however, difficult to model.

To the second category belong the 'top-down' approaches. These subject the spin system, by numerical simulations (*in silico*) or experimentally (on-spectrometer), to a large variety of pulse shapes to optimise the decoupling efficiency. This encompasses the area of optimal control [9], and the method of greatest relevance to this Letter, (e)DUMBO (decoupling using mind-boggling optimisation) [10,11]. DUMBO is the *in silico* optimisation of phase modulated homonuclear decoupling pulse shapes, by simulating the response of a coupled homonuclear two-spin system for a range in dipole–dipole couplings and rf field strengths. The DUMBO method produced a pulse shape whose effectiveness competes with and often outperforms the other methods mentioned above. Unfortunately, understanding the exact mechanism behind the resulting phase modulation is not trivial, as can be expected from a 'top-down' method. DUMBO also has its on-spectrometer implementation named e(xperimental)DUMBO [12], which takes the DUMBO pulse shape as the initial point for a local optimisation, driven by a simplex algorithm. An important advantage of this approach is that the actual spectrometer performance is inherently taken into account. Recently a new version of eDUMBO, named eDUMBO-PLUS [13], was reported for use in the ultra fast MAS regime. Here initial points for local optimisation were found experimentally by a randomised search for well performing phase modulations.

In this Letter, we report a method that simplifies eDUMBO by making the optimisation possible in a single step. We explored the use of a Covariance Matrix Adaptation Evolution Strategies (CMA-ES) algorithm [14] (an evolutionary algorithm), known as a robust many-parameter optimiser, for on-spectrometer optimisation. We report our success in reaching convergence in the whole 12-parameter space spanned by the DUMBO parameterisation. After optimisation, starting from featureless spectra, we confirm the optimal performance of the (e)DUMBO pulse shapes, thereby benchmarking our approach for future work. We chose the adjective EASY-GOING (Evolutionary Algorithms Serving Your Global Optimisation Improvement Needs Gladly), which emphasises the use of evolutionary algorithms which have a broad range of

* Corresponding author.
E-mail address: a.kentgens@science.ru.nl (A.P.M. Kentgens).

0009-2614/$ - see front matter © 2011 Elsevier B.V. All rights reserved.
doi:10.1016/j.cplett.2011.04.079

Table 1
Experimental settings for pulse sequences illustrated in Figure 1. Settings are related to the figure displaying the experimental data. From left to right: spectral width, nutation and rf field offset frequencies in kHz; phase modulation block, phase resolution and acquisition window timings in μs, recycle delay in s and acquisition time in ms.

Figure	sw	ν_{rf}	$\nu_{off}^{^{13}C}$	$\nu_{off}^{^{1}H}$	τ_{pmb}	τ_{res}	τ_{win}	τ_{rd}	τ_{at}
3(a)	33.8	101.4	1.0	−1.0	29.6	0.20	–	3.0	30.0
4(a)	33.8	140.0	–	0.0	25.6	0.25	4.0	2.0	18.0
5	89.3	680.0	–	−2.0	8.8	0.20	2.4	4.0	15.0

applications. The current application is therefore denoted EASY-GOING DUMBO (*EGD*).

To determine the agreement of the experimental results with theory, we simulated the experiments for the optimised phase modulations. The outcomes show that in the current regime of moderate spinning speed and medium rf field strength theory agrees well for these complex pulse shapes. We conclude this Letter by presenting our first results for *EGD* decoupling at very high rf field strengths. To achieve this field strength we used a recently presented micro-magic-angle spinning (μMAS) probehead for application in high-resolution proton solid-state NMR of nanolitre sample volumes [15]. Although this probehead allows to generate proton rf field strengths of 800 kHz with about 10 W of rf power, we found that the optimal proton spectral resolution is achieved at medium rf field strength when using FSLG and (e)DUMBO. We attributed this effect to rf phase transients that scale with the rf field strength [16]. Here we show that our *EGD* approach obtains a pulse sequence that achieves a competitively resolved proton spectrum at very high rf fields.

2. Materials and methods

2.1. Experiment

^{1}H and ^{13}C spectra were recorded on a 300 MHz (7.1 T) Varian NMR spectrometer with VNMRS console and a Bruker 2.5 mm double resonance probe tuned to 300.1 and 75.8 MHz, respectively. The samples were spun at 12.5 kHz in 2.5 mm ZrO_2 spinners. [α-^{13}C,^{15}N] alanine and [^{15}N] glycine samples were purchased from Sigma–Aldrich and used without further purification. The samples were restricted to volumes of approximately 11 μL, so that they reside well within the coil and rf inhomogeneity effects are limited. Experiments reported at very high rf field strength were performed in a recently presented μ-MAS probehead [15]. We performed these experiments on a 400 MHz (9.4 T) Varian spectrometer under 12.5 kHz MAS, additional settings are shown in Table 1. Glycine was held in a fused-silica sample container with an outer diameter of 400 μm and an inner diameter of 320 μm with a sample volume of 70 nL.

Figure 1(a) shows the pulse sequence to obtain *J*-resolved ^{13}C spectra. For every new experiment, during the *EGD* optimisation, a new phase modulated pulse shape is applied while the carbon signal is detected. These experiments were performed on the alanine sample. We used four scans per experiment, and set the length of a phase modulation block τ_{pmb}, determining the rf cycle time τ_c, to correspond to a 6π pulse. Acquisition on the carbon channel was synchronised with this cycle time. Efficient proton–proton decoupling of alanine's CH proton, reveals the splitting caused by the J_{CH}-coupling with the alpha carbon. Further experimental settings are shown in the first row of Table 1.

Figure 1(b) illustrates the pulse sequence for obtaining high-resolution directly detected ^{1}H spectra. The homonuclear decoupling phase modulation is applied between the detection windows. This experiment was carried out on glycine. Efficient decoupling

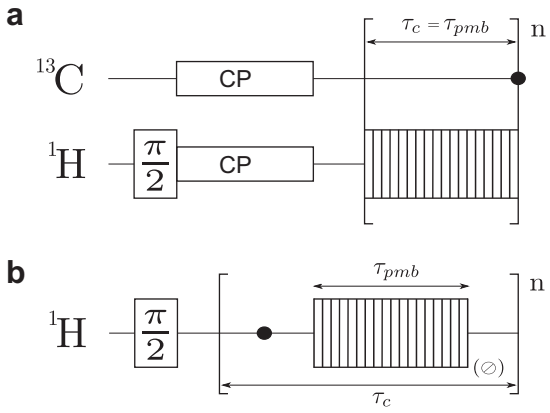

Figure 1. (a) Two-channel pulse sequence for assessing the proton homonuclear decoupling performance via carbon detection. The experiment consists of cross polarisation followed by continuous phase modulation on the proton and acquisition on the carbon channel. The first row in Table 1 displays settings for the performed carbon detection experiments. (b) Single channel pulse sequence employing proton homonuclear decoupling alternated with detection in inserted intervals (windows). ø indicates super cycling with alternating $[0,\pi]$ phase. The second and third row in Table 1 show the experimental settings for the reported proton detection experiments.

will resolve the two lines of the strongly coupled CH_2 protons, making it a reliable indicator of decoupling efficiency. Experimental settings are shown in the second and third row of Table 1. We used four scans per experiment and define the rf cycle time as the sum of the pulse and detection window durations $\tau_c = \tau_{pmb} + \tau_{win}$.

During the experiment, the phase modulation is super cycled to create a *z*-rotation homonuclear decoupling sequence in order to remove zero-frequency contributions from the spectrum without having to optimise an additional pre-pulse prior to the homonuclear decoupling sequence [17]. The orientation of the effective field during the homonuclear decoupling sequence determines the optimal choice of the phase and flip-angle of this pre-pulse to rotate the longitudinal proton magnetisation into a plane that is perpendicular to the effective field resulting in an artifact-free spectrum [17]. This results in a higher scaling factor for the isotropic chemical shift compared to a super cycled sequence, for example DUMBO-1 has a theoretical scaling factor of 0.52 [10], whereas in the super cycled version this reduces to 0.41. However, we chose super cycling to guarantee spectra without artifacts, since the effective field of the homonuclear decoupling sequence is changing during the optimisation of the DUMBO Fourier coefficients, and hence would in principle require to adjust the pre-pulse in each iteration.

The scaling factor of the chemical shift was determined experimentally, as described in [15]. A series of two-dimensional proton spectra were taken as a function of the rf field offset. In these experiments, during t_1 evolution the homonuclear decoupling sequence from Figure 1(b) is applied, while the proton signal is detected in the t_2 domain without decoupling. Analysis of the data is performed by a linear fit of all shifts from the spectra combined in one graph. The slope and offset of this fit are used to correct the proton chemical shifts, by consecutive division and addition, respectively.

2.2. Optimisation strategy

2.2.1. The CMA-ES algorithm

Evolutionary Algorithms (EAs) are based upon the Darwinian theory of a natural selection process occurring by reproduction and mutation of genes in a chromosome leading to only best adapted individuals. The optimisations mentioned in this Letter

were performed with an Evolution Strategy (ES) algorithm, a class of EAs, which start with one or a population of parent(s). A parent is a trial solution, that corresponds to a vector of application and strategy parameters. Application parameters are in this case the Fourier coefficients parameterising the phase modulation. The parent generates offspring in a mutative step-size fashion that depends on the strategy parameters. The fitness (solution performance) of these children is checked and new parents are chosen. There are several different strategies for the generation of the offspring as well as the choice of the next parent(s). For a more detailed description, see [18].

For this work, the CMA-ES algorithm developed by Hansen and Ostermeier [14] was used. In this algorithm the mutative steps are dependent on application-parameter covariance which are determined by taking into account the effect of previous mutations on offspring performance. The algorithm is reported reliable for both local optimisation and global optimisation [19]. The CMA-ES algorithm does not leave the choice of strategy parameters open to the user. The only meta-parameters available are parent and offspring population size.

2.2.2. Algorithm – spectrometer interface

An interface was written to link the CMA-ES algorithm, part of the automated fitting program written by Meerts and Schmitt [20], to the VNMRJ program controlling the spectrometer.

Optimisation parameters of the phase modulation were chosen according to the DUMBO parameterisation [10]

$$\varphi(\tau) = \begin{cases} 0 \leqslant \tau < \frac{1}{2}: & \sum_{n=1}^{6} a_n \cos(2\pi n\tau) + b_n \sin(2\pi n\tau), \\ \frac{1}{2} \leqslant \tau \leqslant 1 \quad : & \varphi(1-\tau) + \pi, \end{cases} \tag{1}$$

with $\tau = \frac{t}{\tau_{pmb}}$ the phase modulation progress, and Fourier coefficients a_n and b_n the optimisation parameters in units of 2π. The discretisation of the phase modulation is determined by the phase resolution τ_{res}, see Table 1. A phase of π is added in the second half of the phase modulation to ensure an rf propagator equal to unity at time τ_{pmb}, at which point the spin operator part of the dipole–dipole Hamiltonian should be averaged to zero. The '$1-\tau$' argument in this part of the phase modulation ensures time reversal symmetry to cancel odd order terms in the Magnus expansion [21]; a property used to reduce simulation complexity in the DUMBO approach.

The quality of the spectrum or induction decay is determined by evaluation of the relevant fitness function. Note that fitness needs to be maximised in analogy to the 'survival of the fittest' concept. For the proton detection experiment this function was defined as the path length the transverse magnetisation travelled in the complex plane

$$\boldsymbol{F} = \sum_{n \in \{b+s,\ldots,b+ms \leqslant N\}} |p_n - p_{n-s}|. \tag{2}$$

Here is N the number of time-domain datapoints, b the index of the starting datapoint, $\frac{1}{s}$ the fraction of spectral width that is observed for the fitness evaluation, m all positive integer values that match the condition $n < N$, and p_n the nth complex datapoint. All presented proton detection experiments are optimised with b equal to three and s equal to six.

The fitness function for the carbon detection experiment was defined as the difference between the average peak intensity of the doublet, and the minimum between the peaks. To ensure a non-zero feedback for the CMA-ES algorithm at all times, one-sixteenth of the maximum spectrum intensity in a pre-set frequency domain was added. For the reported carbon detection experiment the pre-set domain was set to 600 Hz centred at the carrier frequency. This domain was large enough to encompass the width of the expected doublet and to exclude the spectral part not of interest to the optimisation.

2.2.3. Algorithm settings

From the 12 Fourier coefficients in Eq. 1, 11 were allowed to vary from −0.5 to 0.5; the 12th coefficient could only vary over half of this domain. The latter choice excludes phase modulations that only differ by an overall sign change. We observed experimentally that the spectrum does not change by applying $-\varphi(\tau)$ instead of $\varphi(\tau)$.

For the CMA-ES algorithm, a population of 48 with 24 parents and 100 generations was found to be a suitable choice for convergence of the twelve parameter problem. Typical optimisation durations were between 10 and 16 h. Experiments reported here have been done for different random starting populations.

2.3. Simulation

All simulations mentioned, were performed using SPINEVOLUTION [22]. The alanine spin system for the carbon detection experiment, nine protons and one carbon nucleus, was taken from [23], and adjusted by addition of a J_{CH}-coupling of 140 Hz for the alpha carbon. The pulse sequence was matched to the part after CP of Figure 1(a), hence starting with carbon transverse magnetisation. Furthermore, settings according to Section 2.1 were used, including rf cycle synchronised detection.

For simulations of the proton detection experiments on glycine, an effective seven-spin system was setup. Figure 2 illustrates what combinations of nuclei were chosen, to form effective spins that mimic the surrounding direct dipole–dipole couplings to neighbouring glycine molecules. The simulation was setup using the experimental settings of Section 2.1. Simulation started from transverse proton magnetisation and included super cycling. The calculated induction decay proved to be invariant to the choice of detection timepoint in the window. For practical reasons, we then synchronised the detection with the rf cycle time.

In both simulations relaxation was not explicitly taken into account. The simulated induction decays were therefore exponentially apodised. Typical calculation times, for a single spectrum, were between 7 and 10 h on five 2.5 GHz Opteron cores.

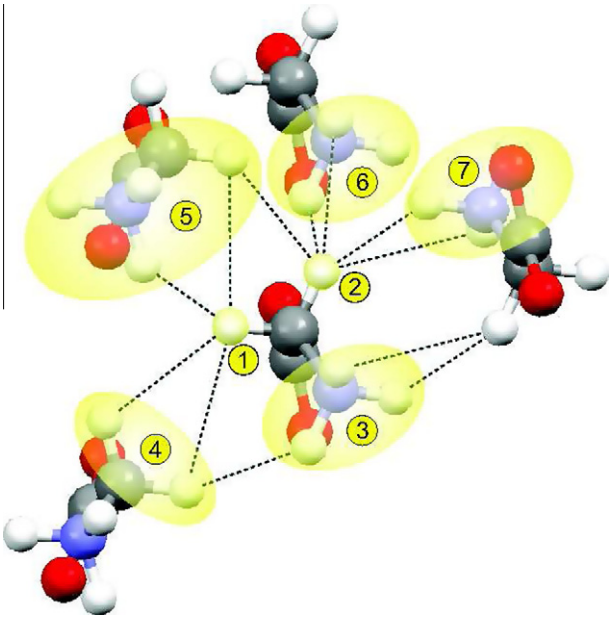

Figure 2. Effective seven-spin system for the glycine simulations.

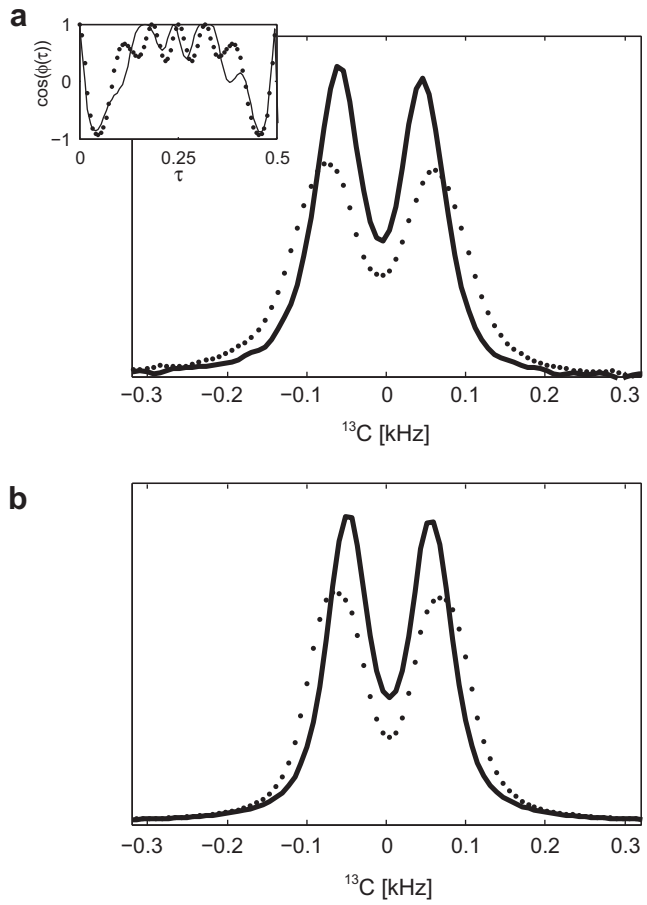

Figure 3. (a) Outcome of *EGD* proton homonuclear decoupling (continuous line) for the carbon detection experiment on [α-^{13}C,^{15}N] alanine. The spectrum and phase modulation are compared to eDUMBO-$1_{12.5}$ data (dotted line). Experimental linewidths at FWHH are Δ(CH) = 68 and 94 Hz, respectively. Phase modulations are shown in the inset, based on the coefficients in Table 2 [12]. (b) Simulation results for the experiment of (a). A spin system consisting of nine protons and one carbon nucleus was used. Simulated induction decays were apodised to match the experiment.

3. Results and discussion

3.1. Optimisation of proton homonuclear decoupling during carbon detection

The outcome of *EGD* optimisation of proton homonuclear decoupling indirectly detected via the carbon signal of [α-^{13}C,^{15}N] alanine, is shown in Figure 3(a). For comparison we added eDUMBO-$1_{12.5}$ data, taken with the same experimental settings as mentioned in Section 2.1.

A comparison of the spectra reveals a better linewidth, but also stronger *J*-coupling scaling for the *EGD* result, so that the effective resolution is about the same. The obtained phase modulations are similar, and it is important to note that the phase modulation coefficients, see Table 2, reaffirm the observation by Elena et al. [12], that cosine coefficients have a negligible contribution. The compromise between scaling of the *J*-splitting and the carbon linewidth makes it difficult to determine which phase modulation performs best. Ultimately, it is the choice of fitness function that determines the outcome. The choice to use the dip-depth of the doublet, appears to be more favourable towards smaller linewidth. Conversely eDUMBO-$1_{12.5}$ is the outcome of using a measure that favours a splitting size equal to the theoretical maximum scaling of 0.57 (for the static-sample case) and maximisation of peak intensities.

Table 2
Coefficients, in units of 2π, found by *EGD* decoupling for the carbon and proton detection experiments.

n	Figure 3(a)		Figure 4(a)		Figure 5	
	a_n	b_n	a_n	b_n	a_n	b_n
1	+0.01911	+0.24799	+0.07188	+0.13788	−0.03859	+0.25292
2	+0.00108	+0.15656	+0.02961	+0.18771	+0.08175	+0.23386
3	+0.01726	+0.10816	+0.06718	+0.01731	+0.26925	−0.15763
4	−0.02958	+0.01289	+0.00219	+0.12842	−0.18227	+0.25675
5	+0.04037	+0.08059	+0.02404	−0.04593	+0.00595	−0.10046
6	−0.03763	−0.00842	+0.04448	+0.05531	–	–

Figure 3(b) shows how simulation is able to predict the trend in scaling of the *J*-coupling for the complex eDUMBO and the *EGD* phase modulations. Apparently the complex pulse shapes have a near ideal behaviour.

3.2. Optimisation of proton homonuclear decoupling during windowed proton detection

Figure 4(a) shows the resulting spectra for employing *EGD* homonuclear decoupling with windowed acquisition of the proton signal. We experimentally determined a scaling factor of 0.56. Data

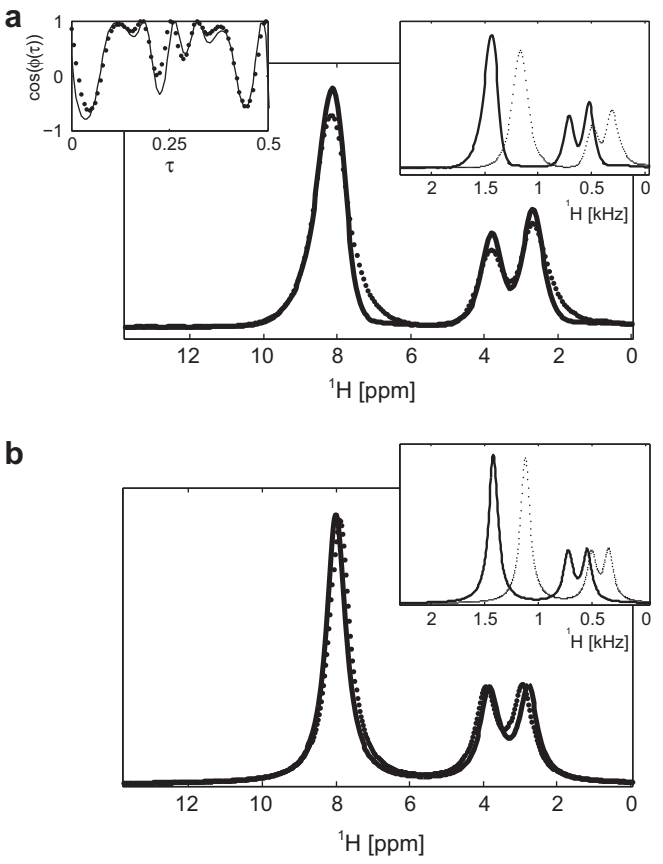

Figure 4. (a) Results for the proton detection experiment on [^{15}N] glycine. Comparison between *EGD* (continuous line) and DUMBO phase modulations and spectra before (inset upper right corner) and after correction for chemical shift scaling (main window). Experimental unscaled linewidths at FWHH are $\Delta(NH_3^+)_{raw}$ = 160, 176 Hz and $\Delta(CH_2)_{raw}$ = 112, 128 Hz and scaled $\Delta(NH_3^+)_{real}$ = 0.95, 1.12 ppm (284, 337 Hz), and $\Delta(CH_2)_{real}$ = 0.67, 0.76 ppm (200, 229 Hz), respectively. Phase modulations, shown in the upper left inset, are based on the coefficients in Table 2 [10]. (b) Simulation of spectra in (a). The effective spin system is illustrated in Figure 2. Simulated induction decays are apodised to match the experimental data.

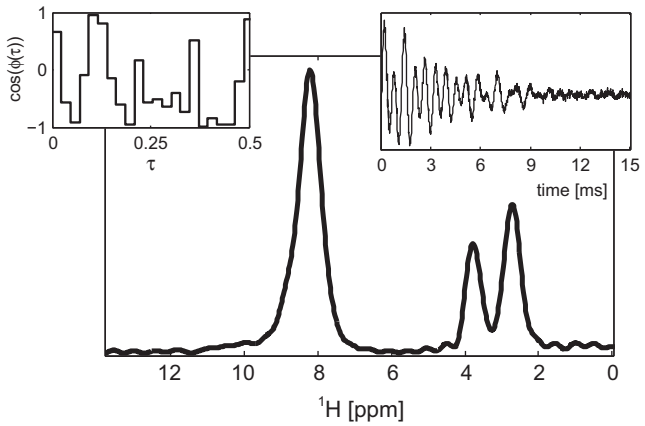

Figure 5. Optimisation outcome for *EGD* proton homonuclear decoupling direct detection experiment at 680 kHz rf field strength, 12.5 kHz MAS on a 400 MHz Varian spectrometer. The phase modulation, coefficients are shown in Table 2, is presented in the inset as stairs to indicate the small amount of phase steps that was used. The experimental spectrum is shown in the main window and its induction decay in the upper right inset. The chemical shift scale of the spectrum was corrected with a scaling factor of 0.32. Experimental unscaled linewidths at FWHH are $\Delta(NH_3^+)_{raw} = 93$ Hz and $\Delta(CH_2)_{raw} = 65$ Hz and scaled $\Delta(NH_3^+)_{real} = 0.73$ ppm (290 Hz) and $\Delta(CH_2)_{real} = 0.51$ ppm (203 Hz), respectively.

obtained by the same experimental settings and the DUMBO phase modulation is displayed in the figure for comparison.

Comparison of the phase modulations shows small deviations, which translate into small discrepancies of the spectra. It is remarkable that our *EGD* phase modulation is so similar to DUMBO, which is obtained *in silico* for a two-spin system. This may be considered as a benchmarking of our method, as discussed below.

Figure 4(b) shows simulation results. We scaled the simulated spectra with the experimental scaling factors. The peak positions as well as the visibility-trend for the CH_2 peaks are reproduced. With the use of the experimental scaling factors for chemical shift correction, a nearly one-to-one mapping of experiment and simulations is obtained. Chemical shift values for spin number one, two and three in Figure 2 were determined from the scaled spectrum in Figure 4(a). It is remarkable that simulations can correctly predict the different outcomes of slightly distinguishable pulse shapes.

The fitness function used for this optimisation seems to be a quite 'natural' choice, no incorporation of unphysical weighting factors, to maximise scaling and minimise linewidth. The path length of the magnetisation in the complex plane becomes longer with increasing dephasing time and if higher or more frequencies are present. This quality factor is also more generally applicable, since it is independent of the number of peaks.

Unfortunately, this fitness function proved to be impractical for optimisation of the proton rf offset. The optimisation will maximise the offset, since that will result in induction decays with faster oscillations. Furthermore, we also applied this fitness function (*b* equal to three and *s* equal to five) for the carbon detection experiment. The resulting spectrum was a singlet. This can be understood by the significantly different dephasing times for an uncoupled and a *J*-coupled carbon nucleus.

3.3. Convergence to (e)DUMBO solutions

Figures 3(a) and 4(a) show that the *EGD* optimisation results at moderate rf field strength resemble those of (e)DUMBO. Especially the results for the proton detection experiment are remarkable; two completely different approaches converge to the same result. We find, viewing the carbon spectra, that the definition of the fitness function can steer the optimisation towards lesser scaling or linewidth. *EGD* experiments performed by us with other fitness functions, for both carbon and proton detection experiments, confirm this observation. From this point of view, the path length fitness function for the proton detection experiment, is a translation of the purely theoretical DUMBO quality measure, into experimental parameters. This is important due to the fact that DUMBO's quality measure is designed for minimising the multi-spin (couplings) and maximising single-spin operator coefficients, an ideal definition for a single-objective (one fitness) optimisation. By the latter statement we would like to refer to the possibility of performing a multi-objective optimisation [24], where the incommensurability of the two objectives can be studied in a more objective sense.

The same search space has been explored by different methods, both *in silico* and on-spectrometer, resulting in similar optima, accepting a difference in measures of quality. This suggests that the one-step *EGD* scheme successfully managed to navigate the 12-parameter search space.

3.4. EASY-GOING DUMBO optimisations at 680 kHz rf field strength

In this section we demonstrate that the *EGD* method is not strongly dependent on the initial choice of parameters, by applying it to new experimental conditions. For this purpose we employed *EGD* homonuclear decoupling at very high rf fields of 680 kHz using our recently presented μMAS setup [15] for high resolution proton NMR. The solenoid coil that generated the strong rf field has an inner diameter of 450 μm and a *Q*-factor of 45.

For the experimental conditions mentioned in Section 2.1, we determined that the DUMBO phase modulation does not resolve glycine's CH_2 peaks. Figure 5 shows the outcome of the *EGD* proton detection experiment at 680 kHz rf field strength. Note that we are applying 12π pulses to ensure the ratio $\frac{\tau_{pmb}}{\tau_{res}}$, equal to 44 in this case, does not become so small that no freedom of choice for the phases is left.

A value of 0.32 was estimated for the experimental scaling factor of the resulting homonuclear decoupling sequence. Although

Table 3
Comparison of experimental parameters and linewidths of the CH_2 resonances for different direct proton detection schemes, including our very high rf field results. All resonances are from glycine except for [13] that used β-L-Asp-L-Ala. From [27] we determined the line width by hand. Columns from left to right represent: reference, sequence name, MAS and rf nutation frequency, main magnetic field strength, scaling factor and, respectively, the scaled linewidth in ppm and Hz, and the unscaled linewidth in Hz.

Ref.	Seq. name	ν_r	ν_{rf}	$\nu_{^1H}$	λ	Δ_{real}		Δ_{raw}
		(kHz)	(kHz)	(MHz)		(ppm)	(Hz)	(Hz)
[13]	PLUS-1	65	170	500	0.73	0.33	165	120
[25]	DUMBO-1	65	170	500	0.47	0.47	230	108
[26]	wPMLG5$^{\bar{x}\bar{x}}_{mm}$	10	99	600	0.47	0.47	282	133
[27]	TIMES	10	170	900	0.35	0.6	550	192
This work	DUMBO-1	12.5	140	300	0.56	0.76	229	128
This work	EASY-GOING DUMBO	12.5	140	300	0.56	0.67	200	112
This work	EASY-GOING DUMBO	12.5	680	400	0.32	0.51	203	65

this scaling is unfavourable, there is a considerable improvement in the linewidth compared to the results depicted in Figure 4(a), exceeding 0.1 ppm. For comparison we tabulated our results together with results for several different direct proton detection methods for homonuclear decoupling in Table 3. This table shows that the unscaled linewidth in Hz for the CH_2 protons obtained in this work compares very favourable to the results published so far. For a well-ordered crystalline compound this line width should be dominated by residual proton–proton dipolar interactions which are efficiently suppressed by *EGD* at high rf field strength which is remarkable, considering the fact that the spectra were obtained under moderate 12.5 kHz MAS on a 400 MHz spectrometer. Unfortunately our scaling factor is unfavourable but still results in a competitive effective resolution as compared to the other methods summarised in Table 3. We therefore anticipate better resolution for *EGD* when implemented at higher external magnetic fields. It certainly encourages further investigation of the potential of very high rf field homonuclear decoupling at higher external fields and/or spinning speeds.

From numerical simulations (not shown) we obtained a scaling factor of 0.22 which does not match the experimental value. We are not certain what causes this discrepancy. Super cycling is able to compensate effects from phase transient that can be described by *z*-rotations [17]. However, our results indicate that this description might no longer be sufficient at high rf fields. Further research is needed to elucidate these effects.

4. Conclusions

We presented the benchmarking and, furthermore, successful application of our one-step EASY-GOING DUMBO phase modulated homonuclear decoupling optimisation scheme at 12.5 kHz MAS conditions. Starting from a random set of phase modulations and featureless spectra we managed to optimise to effective decoupling solutions. Optimisation of proton–proton decoupling at medium rf field strength, for both direct proton and indirect carbon detection schemes, reaffirm the optimal performance of (e)DUMBO, thereby benchmarking our method. Simulations of both experiments reproduce the experimental scaling factors, which shows that theory can distinguish between the influences of slightly differing pulse shapes. We end the Letter with results for EASY-GOING DUMBO optimisation at 680 kHz of rf field strength and 12.5 kHz MAS on a 400 MHz NMR spectrometer. The optimisation resulted in a new pulse shape that provides a competitive spectral resolution, given relatively low MAS and main field requirements. In this case, simulation could not reproduce the scaling factor, for which we do not yet have a sound explanation, given super cycling should compensate for pulse transients. We consider the results at very high rf field strength encouraging for further investigations of the potential of very high rf field homonuclear decoupling.

Acknowledgements

We thank Prof. Dr. Wim J. van der Zande for his chivalrous support of this project. Technicians Jan van Os and Gerrit Janssen are thanked for experimental help as are Dave Rice and Vadim Zorin from Varian Inc. The Netherlands Organisation for Scientific Research (NWO) and Radboud University Nijmegen are acknowledged for their financial support of the solid-state NMR facility for advanced material science.

References

[1] S.P. Brown, Prog. NMR Spectrosc. 50 (2007) 199.
[2] M. Mehring, J.S. Waugh, Phys. Rev. B 5 (1972) 3459.
[3] A. Bielecki, A.C. Kolbert, M.H. Levitt, Chem. Phys. Lett. 155 (1989) 341.
[4] M.H. Levitt, A.C. Kolbert, A. Bielecki, D.J. Ruben, Solid State NMR 2 (1993) 151.
[5] J. Ashida, D. Rice, Magn. Moments 8 (1996) 19. a Varian Publication.
[6] B.M. Fung, K. Ermolaev, Y. Yu, J. Magn. Reson. 138 (1999) 28.
[7] E. Vinogradov, P.K. Madhu, S. Vega, Chem. Phys. Lett. 314 (1999) 443.
[8] P.K. Madhu, X. Zhao, M.H. Levitt, Chem. Phys. Lett. 346 (2001) 142.
[9] N. Khaneja, T. Reiss, C. Kehlet, T. Schulte-Herbrüggen, S.J. Glaser, J. Magn. Reson. 172 (2005) 296.
[10] D. Sakellariou, A. Lesage, P. Hodgkinson, L. Emsley, Chem. Phys. Lett. 319 (2000) 253.
[11] A. Lesage, D. Sakellariou, S. Hediger, B. Eléna, P. Charmont, S. Steuernagel, L. Emsley, J. Magn. Reson. 163 (2003) 105.
[12] B. Elena, G. de Paëpe, L. Emsley, Chem. Phys. Lett. 398 (2004) 532.
[13] E. Salager, J.-N. Dumez, R.S. Stein, S. Steuernagel, A. Lesage, B. Elena-Herrmann, L. Emsley, Chem. Phys. Lett. 498 (2010) 214.
[14] N. Hansen, A. Ostermeier, Evol. Comput. 9 (2001) 159.
[15] A. Brinkmann, S.K. Vasa, H. Janssen, A.P.M. Kentgens, Chem. Phys. Lett. 485 (2010) 275.
[16] A.J. Vega, J. Magn. Reson. 170 (2004) 22.
[17] M. Leskes, S. Steuernagel, D. Schneider, P. Madhu, S. Vega, Chem. Phys. Lett. 466 (2008) 95.
[18] [18] I. Rechenberg, Evolutionsstrategie – Optimierung technischer Systeme nach Prinzipien der biologischen Evolution, Frommann–Holzboog, Stuttgart, 1973.
[19] N. Hansen, S. Kern, in: X. Yao et al. (Eds.), Parallel Problem Solving from Nature PPSN VIII, vol. 3242 of LNCS, Springer, Berlin/Heidelberg, 2004, pp. 282–291.
[20] W.L. Meerts, M. Schmitt, Int. Rev. Phys. Chem. 25 (2006) 353.
[21] U. Haeberlen, High Resolution NMR in Solids. Selective Averaging, Volume Suppl. 1 of Advances in Magnetic Resonance, Academic Press, New York, USA, 1976.
[22] M. Veshtort, R.G. Griffin, J. Magn. Reson. 178 (2006) 248.
[23] J.M. Griffin, C. Tripon, S. Ago, C. Filip, S.P. Brown, Magn. Reson. Chem. 45 (2007) 198.
[24] C.A.C. Coello, Knowl. Inform. Syst. 1 (1999) 269.
[25] E. Salager, R.S. Stein, S. Steuernagel, A. Lesage, B. Elena, L. Emsley, Chem. Phys. Lett. 469 (2009) 336.
[26] M. Leskes, P.K. Madhu, S. Vega, J. Chem. Phys. 128 (2008) 052309.
[27] Z. Gan, P. Madhu, J.-P. Amoureux, J. Trébosc, O. Lafon, Chem. Phys. Lett. 503 (2011) 167.